Semiflexible Polymers in Spherical Confinement: Bipolar Orientational Order Versus Tennis Ball States

Arash Nikoubashman,[1,*] Daniel A. Vega,[2,1] Kurt Binder,[1] and Andrey Milchev[3,1]

[1]*Institute of Physics, Johannes Gutenberg University Mainz, Staudingerweg 7, 55128 Mainz, Germany*
[2]*Department of Physics, Universidad Nacional del Sur-IFISUR-CONICET, 8000 Bahía Blanca, Argentina*
[3]*Institute for Physical Chemistry, Bulgarian Academy of Sciences, 1113 Sofia, Bulgaria*

Densely packed semiflexible polymers with contour length L confined in spheres with radius R of the same order as L cannot exhibit uniform nematic order. Depending on the chain stiffness (which we vary over a wide range), highly distorted structures form with topological defects on the sphere surface. These structures are completely different from previously observed ones of very long chains winding around the inner surface of spheres and from nematic droplets. At high densities, a thin shell of polymers close to the sphere surface exhibits a tennis ball texture due to the confinement-induced gradual bending of polymer bonds. In contrast, when the contour length of the chains is significantly smaller than the radius of the confining sphere, a few bent smectic layers form in the sphere. Molecular dynamics simulations demonstrate these complex structures, and suitable order parameters characterizing them are proposed.

Semiflexible biopolymers such as double-stranded (ds) DNA, actin, microtubules, etc. play a crucial role for structure and function of living matter, and confinement caused by cell membranes is a central aspect in this context [1–3]. For instance, ds DNA packaging in bacteriophage capsids [4–6], storage of chromatin in the cell nucleus, and self-organization of actin filaments in cell-sized confinement [7] are problems motivating appropriate theoretical modeling [8–17]. The majority of previous work focused on the structure formed by a single long macromolecule inside a sphere (in particular, how it is wrapped around the interior surface). However, it is clear that in many contexts high packing densities of anisotropic building blocks are advantageous [11,18]. Such dense packing can be more easily achieved when one confines many semiflexible polymers of intermediate length rather than a single extremely long chain molecule. This problem is also relevant for applications where capsules carry "cargo", with the intention to use triggers to release the enclosed content to achieve the desired action [19], e.g., drug delivery [20]. Some experiments with DNA (or DNA-actin filament mixtures) confined in spherical vesicles [21,22] indeed indicate interesting phase behavior of such systems. We also note analogies as well as differences to the dense packing of stiff short rods inside of spheres [23,24] or in spherical shells [25,26]. It is known that nematic order [27] then is "frustrated" [28] due to topological defects [29–32], and textured smectic shells occur [25,26]. In order to elucidate the complex behavior of semiflexible chains in spherical confinement, we conducted extensive computer simulations.

Since for most cases of interest the sphere radii are of mesoscopic size (0.1–10 μm), atomistically realistic

modeling of semiflexible polymers confined in these spheres is not computationally feasible, and we use instead a coarse-grained bead-spring model [33]. Good solvent conditions are assumed, but the solvent is only implicitly considered via an effective purely repulsive potential $U(r)$ acting between beads at distance r, i.e., $U(r) = 4\varepsilon[(\sigma/r)^{12} - (\sigma/r)^6 + 1/4]$, $r < r_c = 2^{1/6}\sigma$, and $U(r > r_c) = 0$. Here, $\sigma = 1$ and $\varepsilon = 1$ are the units of length and energy, respectively, and will be used in what follows. Neighboring beads along a chain are bonded via an anharmonic spring potential, $U_{\text{spring}} = -(kr_0^2/2)\ln[1 - (r/r_0)^2]$, $r < r_0$, $r_0 = 1.5\sigma$, $k = 30\varepsilon/\sigma^2$. While this model is standard for molecular dynamics (MD) simulations of flexible polymers [40], we also employ a bending potential $U_{\text{bend}}(\Theta_{ijk})$, where Θ_{ijk} is the angle between two successive bonds connecting monomers at positions $\mathbf{r}_i$, $\mathbf{r}_j$ and $\mathbf{r}_k$ ($j = i + 1$, $k = i + 2$)

$$U_{\text{bend}}(\Theta_{ijk}) = \kappa[1 - \cos(\Theta_{ijk})], \tag{1}$$

and κ controls its strength. Using $k_B T = 1$, the length of the bonds is $\ell_b \approx 0.97$, the contour length is $L = (N - 1)\ell_b$ for a chain with N beads, and the persistence length is $\ell_p \approx \kappa \ell_b$. We focus here on rather stiff chains of intermediate length ($N = 32$) confined in spheres with radii comparable to ℓ_p and L, such as $R = 35$. Further, we concentrate on high packing densities $0.2 < \rho < 0.7$ [$\rho = 3\mathcal{N}\sigma^3/(4\pi R^3)$, with total number of beads in the system $\mathcal{N}$]. Surface effects on such confined chains at low densities resemble the behavior at planar repulsive walls, see, e.g., Ref. [41], and will be analyzed elsewhere [42].

The confinement by the (rigid) sphere is described by the same potential as used for the bead-bead repulsion.
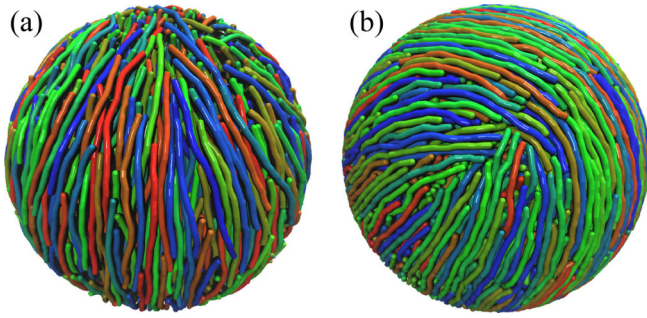
(a)   (b)

FIG. 1.   (a) Snapshot of a system with $N = 32$, $\kappa = 96$ and $\rho = 0.4$ showing bipolar nematic order in a spherical cavity with radius $R = 35$. (b) Tennis ball order at $N = 32$, $\kappa = 32$, and $\rho = 0.7$. Because of the high density of the beads, only chains in the vicinity of the sphere surface are visible. Snapshots rendered using Visual Molecular Dynamics 1.9.2 [48].

This polymer model has been extensively studied in the bulk [43,44] and the isotropic-nematic transition characterized (it occurs for $\rho \approx 0.28$ when $N = \kappa = 32$). Using standard MD methods [43,44] on graphics processing units with the HOOMD-blue code [45–47], we find that the bulk region of the system develops a nematic order from about $\rho \approx 0.27$. At the same time, the surface region of the sphere exhibits bipolar and so-called [12,30,31] tennis ball structures (see Fig. 1).

A rough orientation how these phenomena depend on κ and ρ is derived from a study of the tensor that describes the nematic order in the system,

$$Q_{ni}^{\alpha\beta} = \frac{1}{2}\langle 3\mathbf{u}_{ni}^{\alpha}\mathbf{u}_{ni}^{\beta} - \delta_{\alpha\beta}\rangle, \qquad (2)$$

$\mathbf{u}_{ni}$ being the unit bond vector between monomer i and $i + 1$ for the nth chain, and α, β denoting Cartesian components. Figure 2 shows the three eigenvalues $\lambda_3 > \lambda_2 > \lambda_1$ of the tensor $\bar{Q}^{\alpha\beta}$, where the bar indicates that Eq. (2) is averaged over all bonds in the system. These eigenvalues are zero in fully isotropic solutions, indeed seen for rather flexible chains ($\kappa < 8$), consistent with the bulk behavior of the studied model [43,44]. For $8 \leq \kappa \leq 20$, the chains still can take strongly bent configurations, resulting in a complex partial order. In this stiffness regime, the (local) nematic order is higher in the surface region of the sphere than in its inner part. For $\kappa \geq 32$, however, each chain behaves like a flexible rod, and the (dense) system exhibits considerable order, but it is not similar to the nematic order in the bulk, where $\lambda_3 > 0.5$ and $\lambda_2 \approx 0$ [41,43,44]. Note that for large κ and large ρ, the surface region exhibits a much smaller eigenvalue λ_3 than in the bulk (Fig. 2).

Equilibration of such dense and strongly confined systems as shown in Fig. 2 is notoriously difficult; for the data shown, we started with $\kappa = 96$ and reduced κ gradually. However, using the inverse process, some
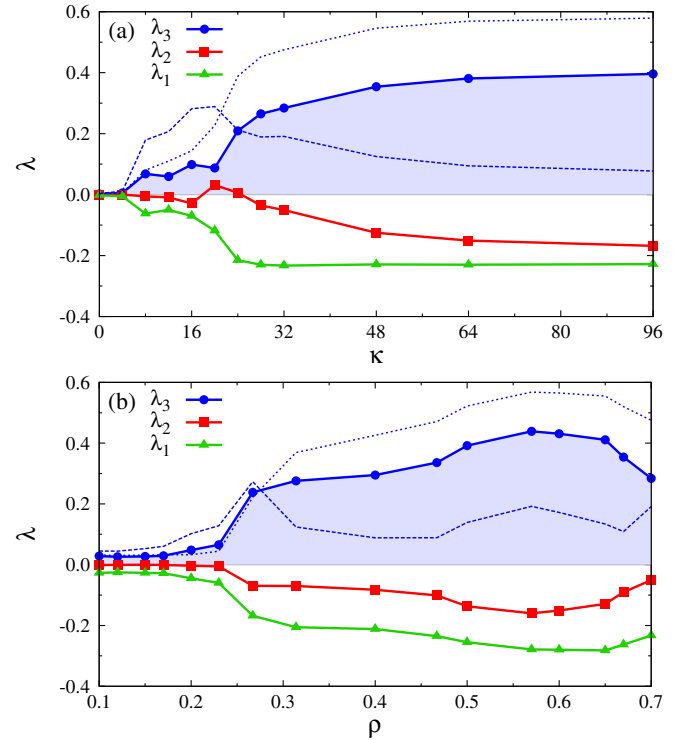

FIG. 2.   Eigenvalues $\lambda_3 > \lambda_2 > \lambda_1$ of the average nematic order parameter of the bonds plotted vs κ at fixed monomer density $\rho = 0.7$ (a) and vs ρ at fixed $\kappa = 32$ (b). Solid lines represent data computed for *all* bonds in the system, whereas dashed and dotted lines correspond to λ_3 of bonds with $r > 0.85R$ (surface shell) and $r < 0.85R$, respectively. $N = 32$ and $R = 35$ here throughout.

hysteresis (near $\kappa = 24$) was found [49]. Such out of equilibrium phenomena may similarly be a problem for real systems.

Radial profiles of the center-of-mass (c.m.) density $\rho_{\text{c.m.}}(r)$ and the chain end monomer density $\rho_E(r)$, as well as the tangential and radial components of the mean square end-to-end vector, $R_{\text{et}}^2(r)$ and $R_{\text{er}}^2(r)$, respectively, yield insight into the structural rearrangement of the chains in the sphere with increasing density (Fig. 3). Here, $\rho_{\text{c.m.}}$ is almost constant throughout the sphere for $\rho < 0.3$, decreasing only for r close to R. For $\rho > 0.3$, both a weak maximum at $r = 0$ and another peak near $r = 32$ develops, indicating that part of the chains gets attached to the sphere surfaces. This layer of surface-attached chains also shows up in the pronounced layering of $\rho_E(r)$. While $R_{\text{et}}^2(r) \approx R_{\text{er}}^2(r) \approx L^2/3$ as long as $r < 12$, $R_{\text{er}}^2(r) \to 0$ for $r \to R$, and then $R_{\text{et}}^2(r)$ is almost $L^2/2$, since then the end-to-end distance has only two tangential components (due to the uniform curvature of wall-attached chains these components are somewhat smaller than $L^2/2$). More interesting is the peak that $\rho_{\text{c.m.}}(r)$ and $R_{\text{er}}^2(r)$ develop for $r \approx L/2$ at high densities (see Fig. 3). This means that chains preferentially gather with their c.m. at a radial distance $r \approx L/2$, and have on average a large projection of their end-to-end distance
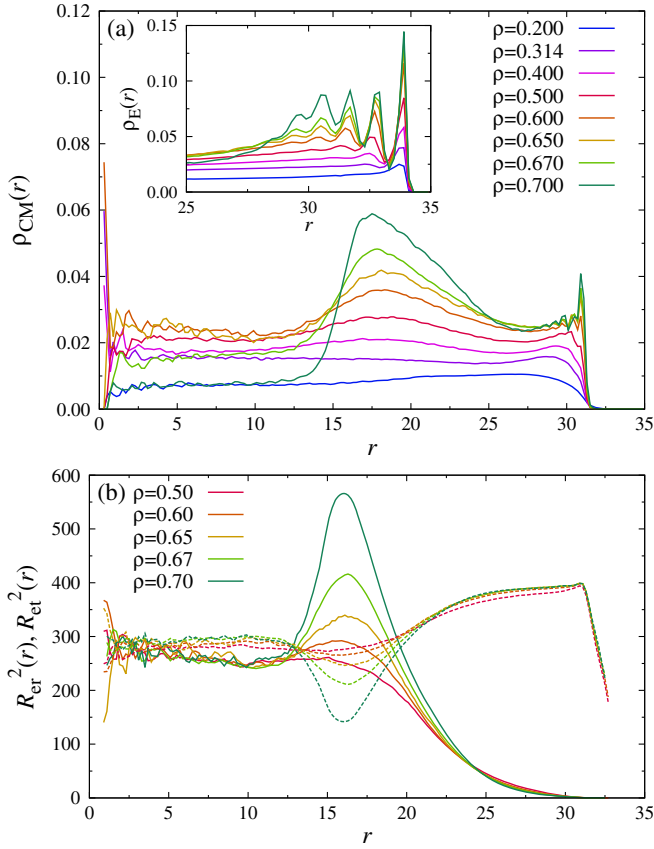
FIG. 3. (a) Radial profile of the center-of-mass density $\rho_{c.m.}(r)$ of semiflexible polymers with $N = \kappa = 32$ in a sphere of radius $R = 35$, for various densities ρ. Decreasing density from top to bottom at $r = 17.5$. Inset shows the end monomer density $\rho_E(r)$ close to the wall. (b) Mean square radial [$R_{er}^2(r)$, solid] and tangential [$R_{et}^2(r)$, dashed] components of the end-to-end distance for chains with center of mass at a distance r from the sphere center for various ρ.
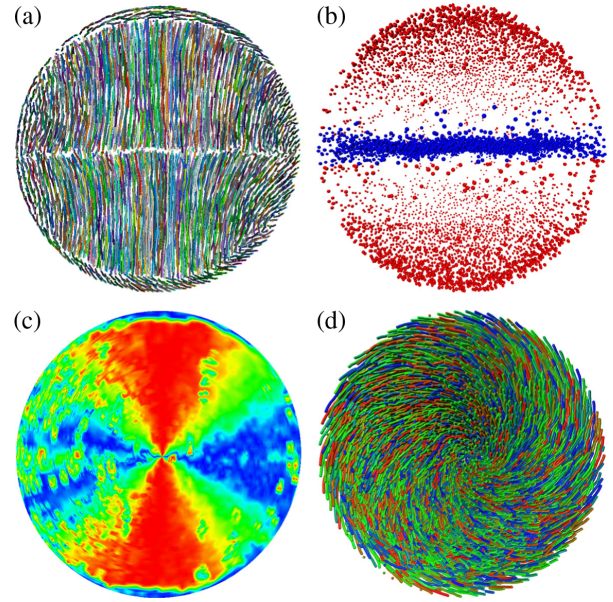
FIG. 4. (a) Slice perpendicular to the equatorial plane. Different chains are shown with different colors simply to allow an easier identification. Each chain that has one end close to the equatorial plane has the other one close to the sphere surface, which requires a considerable splay deformation of the nematic order. (b) Snapshot picture showing chain ends only (ends defining the equatorial plane are shown in blue, the others in red). The "disk" formed by the blue points has a radius of about 32.4, and the eigenvalues of the associate gyration tensor are $\Lambda_3 = \Lambda_2 = 262 \pm 3$, $\Lambda_1 = 2.6 \pm 0.1$. (c) Same as (a) but plotting the radial component of the director field in the zy plane perpendicular to the equatorial plane. The color gradient indicates the degree of bond-vector orientation along this field (red: full; blue: zero). (d) View on one of the hemispheres from the center of the sphere to one of the poles. All data for $N = 32$, $\kappa = 96$, and $\rho = 0.7$.

on the radius vector. This behavior appears only for $\rho > 0.5$, and then exhibits also a pronounced peak at small r [49].

This structural transition can be explained by an accumulation of chain ends in a particular equatorial plane of the cavity. Whenever such a plane exists, the location and orientation of it can be identified through the eigenvalues ($\Lambda_3 > \Lambda_2 > \Lambda_1$) and corresponding eigenvectors of the gyration tensor of all the chain ends (with $r < 0.5R$, to safely exclude those located in the surface shell). The large asphericity $\alpha_\Lambda = \Lambda_3 - (\Lambda_2 + \Lambda_1)/2 > 60$ for $0.5 \leq \rho \leq 0.7$ indicates an accumulation of chain ends in a plane [49], the normal vector $\mathbf{n}$ belonging to the smallest eigenvalue Λ_1. This structure is visualized in Figs. 4(a)–(d). An interesting aspect is the whirl-like arrangement of the chains on the surface, strongly correlated with the appearance of an equatorial (xy) plane.

Figure 4 implies that bonds are aligned almost perpendicular to the equatorial (xy) plane when their distance z from this plane is small, but the chains are

increasingly twisted as they approach the sphere surface. To quantify this effect, we define the order parameter S [12],

$$S(r) = \frac{1}{M} \sum_{i=1}^{M} \cos(2\vartheta_i), \tag{3}$$

ϑ_i being the angle that a bond $\mathbf{u}_{ni}$ makes with respect to a "latitude circle" around the z axis in a concentric spherical shell $[r, r + \delta r]$, and M being the number of bonds in the shell. $S = -1$ means that bonds are parallel to the z axis and $S = +1$ means they are parallel to the "latitude circle." Figure 5(a) shows that $S(r)$ is negative for most densities, whereas positive $S(r)$ only occurs for $\rho \geq 0.67$ near the sphere surface. Further, $S(r)$ is almost -1 for small r, while for $0.5 < \rho < 0.7$ only $S(r < 10) \approx -0.7$ is reached. In all cases, we find a very gradual and systematic change of $S(r)$ with r throughout the sphere.

Finally, we introduce an order parameter suitable to distinguish between the bipolar and tennis ball character of defects in the surface layer. We define a tensor
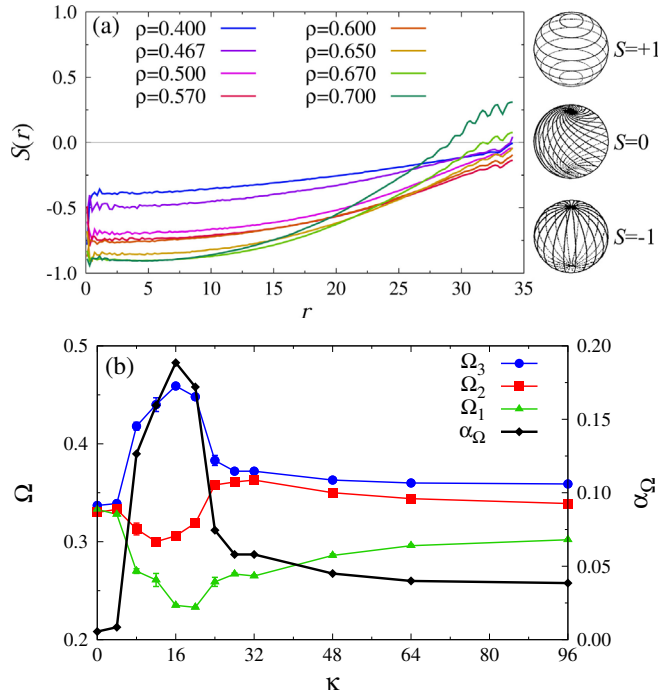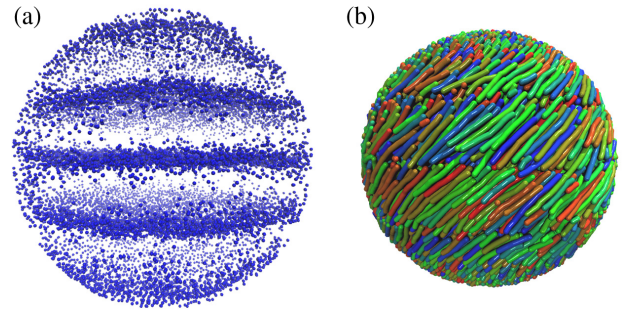
FIG. 6. (a) Snapshot of chain ends for the case of short chains with $N = 16$, $\kappa = 48$, $\rho = 0.7$, and $T = 0.6$. Three distinct layers of ends are visible. (b) Snapshot of chains with $r < 0.85R$ at the same state point, demonstrating the smectic order in the inner part of the sphere. Snapshots in (a) and (b) are drawn at the same scale.

FIG. 5. (a) $S(r)$ plotted vs r for the case $\kappa = 32$ at various densities ρ as indicated. Increasing density from top to bottom at $r = 5$. Schematics adapted from Ref. [50]. (b) Eigenvalues of the tensor Ω (left axis) and its asymmetry α (right axis) for various κ at fixed $\rho = 0.7$. $N = 32$ and $R = 35$ here throughout.

$$\Omega = \frac{1}{M-1} \sum_{i=1}^{M-1} \left(\frac{\mathbf{u}_i \times \mathbf{u}_{i+1}}{|\mathbf{u}_i \times \mathbf{u}_{i+1}|} \right) \otimes \left(\frac{\mathbf{u}_i \times \mathbf{u}_{i+1}}{|\mathbf{u}_i \times \mathbf{u}_{i+1}|} \right), \quad (4)$$

for all bonds which lie between $0.85R < r < R$. Each unit vector defined by the parentheses in Eq. (4) defines a plane, in which two subsequent bonds lie [12]. Averaging the tensor components of Ω over all bonds and diagonalizing, the eigenvalues and eigenvectors for the entire system are obtained. In the disordered case, we found $\Omega_3 \approx \Omega_2 \approx \Omega_1$ for the three eigenvalues of Ω. For the bipolar case, we found $\Omega_3 > \Omega_2 > \Omega_1$, where the eigenvector $\mathbf{n}_{pol}$ belonging to the smallest eigenvalue, Ω_1, provides a good description for the location of the poles. For the quadrupolar tennis ball configuration, we found $\Omega_3 \approx \Omega_2 > \Omega_1$. The transition between these three states can also be identified via the asymmetry $\alpha_\Omega = \Omega_3 - (\Omega_2 + \Omega_1)/2$. Figure 5(b) presents Ω and α_Ω for a system with $\rho = 0.7$ at various κ, clearly showing the disordered-bipolar and bipolar-tennis ball transitions at $\kappa = 8$ and $\kappa = 24$, respectively. The analogous analysis at fixed $\kappa = 32$ for varying density is more challenging, as the polymer density in the surface region becomes rather low at small ρ [cf. inset of Fig. 3(a)]. Nevertheless, we were able to identify a distinct tennis ball structure for $\rho \geq 0.4$. Interestingly, the bulk region beneath the surface exhibits a bipolar nematic order, which gradually twists into the tennis ball texture as the confinement is approached.

In conclusion, the competition between nematic order and confinement of (rather stiff) semiflexible polymers of contour length L in a sphere of radius R comparable to L at rather large densities leads to complicated nonuniform structures. At intermediate densities, the ordering is of nematic type with bipolar defects, and although a significant fraction of the chains occurs in a dense surface-attached layer, near-surface order is still controlled by the order in the sphere interior. At somewhat higher densities, the character of the bulk order changes, and an equatorial plane appears with chains having one chain end close to this plane, the other close to the sphere surface. This structure can be viewed as a caricature of smectic order inside the sphere; in fact, when we choose L considerably smaller than R, see Fig. 6, then we find that several parallel planes where chain ends accumulate appear, confirming this interpretation. In this case, the average nematic director still coincides with the z axis normal to the equatorial planes, and the surface order is compatible with the bulk. For the largest densities accessible in our work, the surface layer ordering develops features differing from the interior, showing tennis ball-like textures, so far seen only when single, very long semiflexible polymers are confined to the surface of spheres. Understanding all these unconventional ordered structures should be helpful for suitable applications of such strongly confined polymeric systems, and could give insight into related phenomena in biological systems. In addition, the "patchiness" provided by the topological defects on the sphere surface can have important implications in the use of anisotropic nanoparticles as building blocks for colloidal self-assembly [18].

---

*anikouba@uni-mainz.de

[1] B. Alberts, A. Johnson, J. Lewis, M. Raff, K. Roberts, and P. Walker, *Molecular Biology of the Cell* (Garland Science, New York, 2007).

[2] M. R. Mofrad and R. Kamm, *Cytoskeletal Mechanics* (Cambridge University Press, Cambridge, England, 2006).

[3] M. Miyazaki, M. Chiba, H. Eguchi, T. Ohki, and S. Ishiwata, Nat. Cell Biol. **17**, 480 (2015).

[4] W. Earnshaw and S. Harrison, Nature (London) **268**, 598 (1977).

[5] M. Cerritelli, N. Cheng, A. Rosenberg, C. McPherson, and A. Steven, Cell **91**, 271 (1997).

[6] E. Katzav, M. Adda-Bedia, and A. Boudaoud, Proc. Natl. Acad. Sci. U.S.A. **103**, 18900 (2006).

[7] M. Soares e Silva, J. Alvarado, J. Nguyen, N. Georgouilla, B. Mulder, and G. Koenderin, Soft Matter **7**, 10631 (2011).

[8] T. Sakaue, Macromolecules **40**, 5206 (2007).

[9] G. Morrison and D. Thirumalai, Phys. Rev. E **79**, 011924 (2009).

[10] K. Ostermeir, K. Alim, and E. Frey, Soft Matter **6**, 3467 (2010).

[11] N. Stoop, J. Najafi, F. K. Wittel, M. Habibi, and H. J. Herrmann, Phys. Rev. Lett. **106**, 214102 (2011).

[12] W.-Y. Zhang and J. Chen, Europhys. Lett. **94**, 43001 (2011).

[13] C. Micheletti, D. Marenduzzo, and E. Orlandini, Phys. Rep. **504**, 1 (2011).

[14] D. Reith, P. Cifra, A. Stasiak, and P. Virnau, Nucleic Acids Res. **40**, 5129 (2012).

[15] D. Marenduzzo, C. Micheletti, E. Orlandini, and D. Sumners, Proc. Natl. Acad. Sci. U.S.A. **110**, 20081 (2013).

[16] M. Fošnarič, A. Iglič, D. M. Kroll, and S. May, Soft Matter **9**, 3976 (2013).

[17] J. Gao, P. Tang, Y. Yang, and J. Z. Y. Chen, Soft Matter **10**, 4674 (2014).

[18] S. C. Glotzer and M. J. Solomon, Nat. Mater. **6**, 557 (2007).

[19] H. N. Yow and A. F. Routh, Soft Matter **2**, 940 (2006).

[20] W. Qi, X. Yan, J. Fei, A. Wang, Y. Cui, and J. Li, Biomaterials **30**, 2799 (2009).

[21] A. Kato, E. Shindo, T. Sakaue, A. Tsuji, and K. Yoshikawa, Biophys. J. **97**, 1678 (2009).

[22] M. Negishi, T. Sakaue, K. Takiguchi, and K. Yoshikawa, Phys. Rev. E **81**, 051921 (2010).

[23] Y. Trukhina and T. Schilling, Phys. Rev. E **77**, 011701 (2008).

[24] I. Gârlea, P. Mulder, J. Alvarado, O. Dammone, D. Aarts, M. Lettinga, G. Koenderink, and B. Mulder, Nat. Commun. **7**, 12112 (2016).

[25] T. Lopez-Leon, A. Fernandez-Nieves, M. Nobili, and C. Blanc, Phys. Rev. Lett. **106**, 247802 (2011).

[26] O. Manyuhina and M. Bowick, Int. J. Non Linear Mech. **75**, 87 (2015).

[27] P. G. de Gennes and J. Prost, *The Physics of Liquid Crystals*, 2nd ed. (Clarendon, Oxford, England, 1992).

[28] T. Lopez-Leon, V. Koning, K. Devaiah, V. Vitelli, and A. Fernandez-Nieves, Nat. Phys. **7**, 391 (2011).

[29] M. Kleman, L. Michel, and G. Toulouse, J. Phys. Lett. **38**, 195 (1977).

[30] D. R. Nelson, Nano Lett. **2**, 1125 (2002).

[31] V. Vitelli and D. R. Nelson, Phys. Rev. E **74**, 021711 (2006).

[32] M. Kleman and O. Lavrentovich, Philos. Mag. **86**, 4117 (2006).

[33] See Supplemental Material at http://link.aps.org/supplemental/10.1103/PhysRevLett.118.217803, which includes Refs. [34–39], for technical details and an exemplary mapping to dsDNA.

[34] J. D. Weeks, D. Chandler, and H. C. Andersen, J. Chem. Phys. **54**, 5237 (1971).

[35] M. Bishop, M. H. Kalos, and H. L. Frisch, J. Chem. Phys. **70**, 1299 (1979).

[36] K. Kremer and G. S. Grest, J. Chem. Phys. **92**, 5057 (1990).

[37] J. Kindt, S. Tzlil, A. Ben-Shaul, and M. Gelbart, Proc. Natl. Acad. Sci. U.S.A. **98**, 13671 (2001).

[38] M. P. Allen and D. J. Tildesley, *Computer Simulation of Liquids* (Clarendon Press, Oxford, England, 1989).

[39] D. C. Rapaport, *The Art of Molecular Dynamics Simulation*, 2nd ed. (Cambridge University Press, Cambridge, England, 2004).

[40] G. S. Grest and K. Kremer, Phys. Rev. A **33**, 3628 (1986).

[41] S. A. Egorov, A. Milchev, P. Virnau, and K. Binder, J. Chem. Phys. **144**, 174902 (2016).

[42] A. Milchev, S. A. Egorov, A. Nikoubashman, and K. Binder, J. Chem. Phys. **146**, 194907 (2017).

[43] S. A. Egorov, A. Milchev, and K. Binder, Phys. Rev. Lett. **116**, 187801 (2016).

[44] S. A. Egorov, A. Milchev, P. Virnau, and K. Binder, Soft Matter **12**, 4944 (2016).

[45] J. A. Anderson, C. D. Lorenz, and A. Travesset, J. Comput. Phys. **227**, 5342 (2008).

[46] J. Glaser, T. D. Nguyen, J. A. Anderson, P. Lui, F. Spiga, J. A. Millan, D. C. Morse, and S. C. Glotzer, Comput. Phys. Commun. **192**, 97 (2015).

[47] http://codeblue.umich.edu/hoomd-blue (v.1.3.3).

[48] W. Humphrey, A. Dalke, and K. Schulten, J. Mol. Graphics **14**, 33 (1996).

[49] See Supplemental Material at http://link.aps.org/supplemental/10.1103/PhysRevLett.118.217803 for more information.

[50] J. Bezić and S. Žumer, Liq. Cryst. **11**, 593 (1992).